Available online at www.sciencedirect.com
SCIENCE DIRECT®
Journal of Nuclear Materials 343 (2005) 197–204
journal of nuclear materials
www.elsevier.com/locate/jnucmat

DPA calculation for Japanese spallation neutron source

M. Harada [a,*], N. Watanabe [a], C. Konno [a], S. Meigo [a], Y. Ikeda [a], K. Niita [b]

[a] Japan Atomic Energy Research Institute, Neutron Facility Group, Centre for Proton Accelerator Facility, 2-4 Shirataka-shirane, Tokai-mura, Naka-gun, Ibaraki 319-1195, Japan
[b] Research Organization for Information Science and Technology, Tokai-mura, Naka-gun, Ibaraki, 319-1106, Japan

Abstract

A neutron generating target and surrounding components, such as moderators and proton-beam windows, of intense pulsed spallation sources suffer serious radiation damage. In order to construct a maintenance scenario of the Japanese Spallation Neutron Source, the life estimation of those components due to the radiation damage becomes indispensable. For this purpose, we calculated DPA values of the important components, based on the calculation of displacement cross-sections using PHITS and NJOY codes with the LA150 library. Maximum DPA values at the end of 5000 MW h are 3.9 for the target vessel, 2.8 for the reflector and moderator vessels, and 0.4 for the proton-beam window. We also discuss the effect of the proton-beam profile and proton-energy dependence on the DPA values. Briefly, we showed the calculation result on the helium and hydrogen production.

1. Introduction

Japanese Spallation Neutron Source (JSNS) is being constructed as one of the major facilities in Japan Proton Accelerator Research Complex (J-PARC). As major components of the source, which are susceptible to serious radiation damage, JSNS has a proton-beam window and vessels for a mercury target, three super-critical hydrogen moderators and a reflector. 1 MW proton beam (3 GeV and 25 Hz) hits the mercury target and slow neutrons are extracted from these moderators for neutron scattering experiments. Vessels and windows of these components suffer the most serious radiation damage. 316L stainless steel will be used as a target vessel material and aluminum alloy A5083 for the proton-beam window. For moderator and reflector vessels, aluminum alloy A6061-T6 will be used. For the construction of a maintenance scenario, the life estimation of those structure materials becomes indispensable. Therefore, we need to evaluate DPA (displacement per atom) value of each component, since DPA is a major index of the radiation damage.

For DPA calculations, flux data calculated by a particle transport code and displacement cross-sections of each element are necessary. To realize a general purpose particle and heavy-ion transport code system, PHITS [1] (Particle and Heavy Ion Transport code System) has been developed by the collaboration of Tohoku University, Japan Atomic Energy Research Institute and Research Organization for Information Science & Technology. PHITS is based on a high-energy hadron transport code, NMTC/JAM [2], and combined with a low-energy transport code, MCNP-4C [3]. Therefore, PHITS is equipped with a low-energy capability in addition to a high-energy one, covering from thermal to

* Corresponding author. Tel.: +81 29 282 6217; fax: +81 29 282 6496.
E-mail address: harada@cens.tokai.jaeri.go.jp (M. Harada).

0022-3115/$ - see front matter © 2005 Elsevier B.V. All rights reserved.
doi:10.1016/j.jnucmat.2005.01.023

high-energy. A function to calculate the displacement cross-sections has been introduced in NMTC/JAM [4]. Recently, we implanted a DPA calculation function in PHITS. With this new PHITS, it becomes possible to perform DPA calculations without successive calculations using two different code systems as NMTC/JAM and MCNP-4 C.

In this paper, we discuss the calculated displacement cross-sections and report calculated values of DPA with DPA maps. The production of hydrogen, helium and silicon is also briefly shown. We also discuss the effect of the proton-beam profile and the proton-energy dependence on DPA.

2. Calculation method of DPA and calculated displacement cross-section

2.1. Calculation method of DPA

DPA calculations can be archived from the following equation:

$$\mathrm{DPA} = \left(\int \sigma_{\mathrm{DX}}(E) \cdot \phi(E) \cdot \mathrm{d}E \right) \cdot t, \tag{1}$$

where $\sigma_{\mathrm{DX}}(E)$ is the displacement cross-section for an incident particle at an energy E, $\phi(E)$ the incident particle flux of protons or neutrons and t the irradiation time. To perform DPA calculations using Eq. (1), $\sigma_{\mathrm{DX}}(E)$ must be determined. For neutrons in the energy range where evaluated cross-section libraries are available, $\sigma_{\mathrm{DX}}(E)$ were processed by the NJOY code [5] with the HEATR modules and an evaluated library. Above the energy range where no available evaluated library exists, $\sigma_{\mathrm{DX}}(E)$ for neutrons and protons were calculated using energies of fragments obtained by PHITS.

In general, $\sigma_{\mathrm{DX}}(E)$ can be obtained from the following equation,

$$\sigma_{\mathrm{DX}}(E) = \sum_i \int_{T_{\mathrm{d}}}^{T_{\max}} \nu_{\mathrm{d}}(T) \cdot \frac{\mathrm{d}\sigma_{\mathrm{d}}^i(T,E)}{\mathrm{d}T} \cdot \mathrm{d}T, \tag{2}$$

where T is the PKA energy, $T_{\max}$ the maximum of T, T_{d} the atomic threshold displacement energy. $\nu_{\mathrm{d}}(T)$ the displacement damage function. $\frac{\mathrm{d}\sigma_{\mathrm{d}}^i(T,E)}{\mathrm{d}T}$ the energy-differential cross section to be T at E for i-th element. The values of $\frac{\mathrm{d}\sigma_{\mathrm{d}}^i(T,E)}{\mathrm{d}T}$ can be calculated by PHITS and NJOY with the evaluated library.

$\nu_{\mathrm{d}}(T)$ is expressed by the following equation [6],

$$\nu_{\mathrm{d}}(T) = \left(\frac{\beta}{2T_{\mathrm{d}}} \right) \cdot T_{\mathrm{dam}}, \tag{3}$$

where β is the constant of 0.8 [6]. T_{dam} the damage energy.

The important parameters necessary to calculate $\sigma_{\mathrm{DX}}(E)$ are listed in Table 1 for elemental materials used.

Table 1
Important parameters necessary to calculate $\sigma_{\mathrm{DX}}(E)$

Material	Atomic displacement energy in NJOY[a] T_{d} (eV)	Atomic displacement energy in PHITS[b] T_{d} (eV)	Low limit energy in PHITS (MeV)
Be	31	40	25
C	31	40	155
Al	27	25	155
Cr	40	40	155
Fe	40	40	155
Ni	40	40	155
Cu	40	30	155
Pb	25	25	155

[a] These are default values in NJOY.
[b] These are taken from Ref. [7].

Values of T_{d} [7] used in PHITS and NJOY are also listed in Table 1. For the $\sigma_{\mathrm{DX}}(E)$ calculation, we can utilize existing cross-section library below 20 MeV. The LA 150 library [8] can be used up to 150 MeV. For the values of T_{dam}, Lindhard–Robinson model [6,9] is used in PHITS.

2.2. Calculated displacement cross-section

As an example of $\sigma_{\mathrm{DX}}(E)$, Fig. 1 shows calculated values of $\sigma_{\mathrm{DX}}(E)$ of ^{56}Fe for neutrons using various codes and libraries [4,10]. In an energy range from 20 MeV to 150 MeV, the DPA values for neutrons calculated by PHITS and LAHET [11] are lower than those by NJOY with LA 150. It is known that, at lower ener-

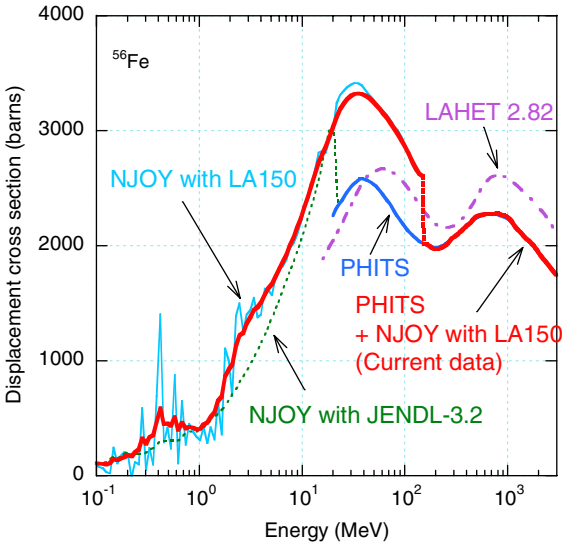

Fig. 1. Comparison of displacement cross-sections of ^{56}Fe for neutrons. All curves are smoothed.

gies (<150 MeV), the nuclear reaction model used in PHITS was not in good agreement with experimental data [12]. On the other hand, calculations of neutron spectra with LA 150 gave fairly good agreement with measurements [12]. Therefore, we adopted the DPA values for neutrons below 150 MeV obtained by NJOY with LA150. However, for neutrons above 155 MeV and for proton in all energies we adopted the results obtained with PHITS, because there is no available library for neutron above 1 GeV (up to 1 GeV, BISERM-2 library [13] is available). One important advantage of PHITS is the capability to obtain DPA in high-energy region above 150 MeV directly.

We considered that the difference between the calculated $\sigma_{DX}(E)$ with PHITS and LAHET was due to the difference in reaction cross sections [14] and nuclear models. As already mentioned, the high-energy part of PHITS is essentially same as NMTC/JAM, which has already been validated in various applications [15–18]; for example, calculations on double differential cross sections of neutron emission from a lead target bombarded by 3 GeV proton compared with measurements [2]. There is another comparison between calculation and measurement for those cross-sections bombarded by 800 MeV protons [15]. Calculation by INC/GEM gave better agreement with measurement than by LAHET. INC code is almost same as the Bertini code, which are included in both PHITS (NMTC/JAM) and LAHET. One of differences between PHITS (NMTC/JAM) and LAHET is with GEM and without. Therefore, we think that PHITS has been validated also in the application.

The lowest energy limit to apply $\sigma_{DX}(E)$ obtained with PHITS was 155 MeV. We connected σ_{DX} ($E = 155$ MeV) with PHITS to σ_{DX} ($E = 150$ MeV) obtained with LA150 (using NJOY) by straight line (broken line in Fig. 1). Fig. 2 shows $\sigma_{DX}(E)$ of ^{27}Al and ^{56}Fe for neutrons and protons using PHITS combined with the LA150 library as mentioned above. $\sigma_{DX}(E)$ of ^{27}Al and ^{56}Fe for neutrons are higher than those for proton up to about 150 and 300 MeV, respectively, being almost the same beyond these energies. $\sigma_{DX}(E)$ of ^{27}Al are lower than those of ^{56}Fe at $E > 8$ MeV for neutrons and $E > 20$ MeV for protons, while higher than the latter below these energies.

$\sigma_{DX}(E)$ for alloys were obtained by linear combinations of $\sigma_{DX}(E)$ of each element of the alloys. As an example, Fig. 3 shows those for 316L stainless steel obtained with procedure mentioned above, compared with those for ^{56}Fe.

To obtain more precise DPA, we have to take into account the effect of the Rutherford scattering of protons. Note that the Rutherford scattering is not included in PHITS. We calculated $\sigma_{DX}(E)$ for protons including the Rutherford scattering. We calculated $\sigma_{DX}(E)$ for protons including the Rutherford scattering using the equation in the reference [19]. The result is shown in Fig. 4.

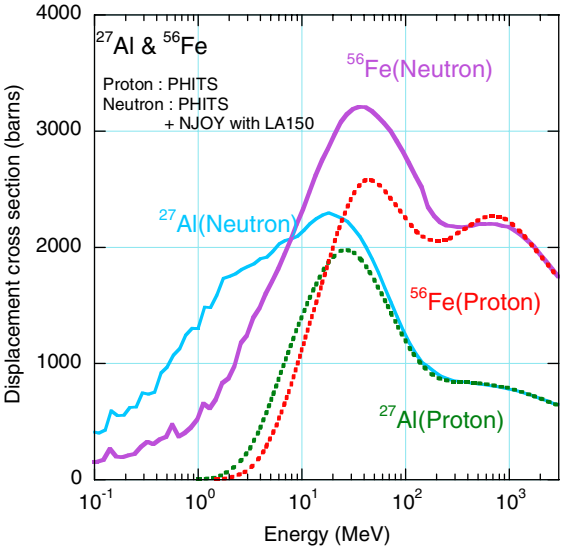

Fig. 2. Displacement cross-sections of ^{27}Al and ^{56}Fe for neutrons and protons.

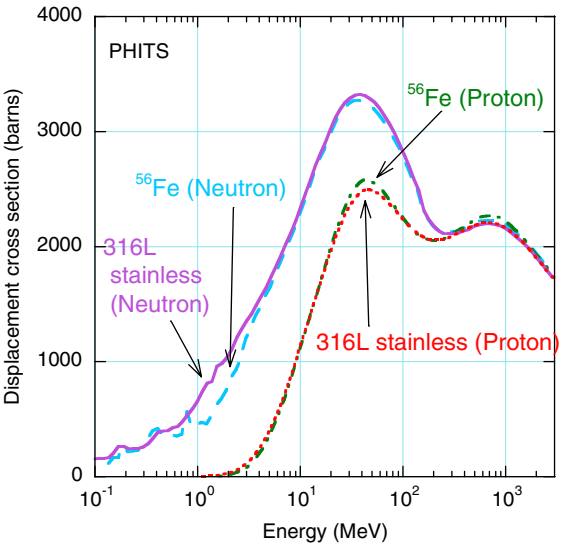

Fig. 3. Displacement cross-sections of 316L stainless steel and ^{56}Fe for neutrons and protons.

3. Calculation model and calculated results of DPA

3.1. Calculation model

Fig. 5 shows a calculation model used for the present study. This is very close to an engineering model. The main parameters of the source are summarized in Table 2.

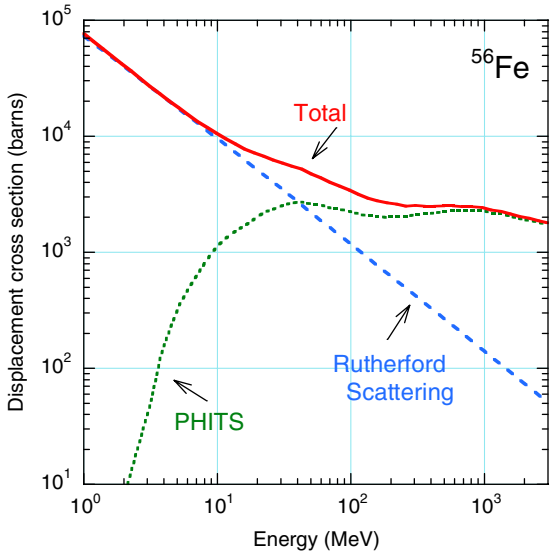

Fig. 4. Displacement cross-sections by the Rutherford scattering of ^{56}Fe for protons.

We assumed three different proton-beam profiles in real space as shown in Fig. 6. Originally we assumed a Gaussian profile in phase space with a small footprint (13×5 cm^2, case 1), but we found that an unacceptable pressure wave effect appeared on the mercury target container vessel [20]. Therefore, we improved the profile to a uniform in phase space with the unchanged beam footprint (13×5 cm^2, case 2) resulting in still unacceptable level in the pressure wave. As a more practical profile based on the various experiences, we finally assumed a profile consisting of a uniform core part and a Gaussian halo part with an expanded footprint (18×7 cm^2, case 3) to reduce the pressure effect to an acceptable level.

Fig. 7 shows proton and neutron spectra at the proton-beam window, the front windows of mercury container vessel and the reflector vessel (at maximum DPA region). DPA in these regions were calculated using the proton and neutron fluxes shown in Fig. 7.

3.2. Calculated DPA

The calculated maximum DPA values for major components are listed in Table 3. We obtained the maximum DPA values at the end of the 5000 MW h operation (5000 h/y at 1 MW) to be 3.9 for the target container vessel, 2.8 for the reflector and moderator vessels, and 0.4 for the proton-beam window, respectively. Note that the effect of Rutherford scattering on DPA is small as listed in the sixth column of Table 3 (not counted to the total value), although the value of $\sigma_{DX}(E)$ for the Rutherford scattering at lower proton energy is monotonically increasing with decreasing proton energy. This is because the energy spectrum of proton is rapidly decreasing at lower energies (see Fig. 7).

Design lives of the major components are listed in the fourth column of Table 4. Note that the design life is not determined only by the radiation damage (DPA) but also other factors: for example in case of decoupled moderators, the lives of decouplers and a poison are also

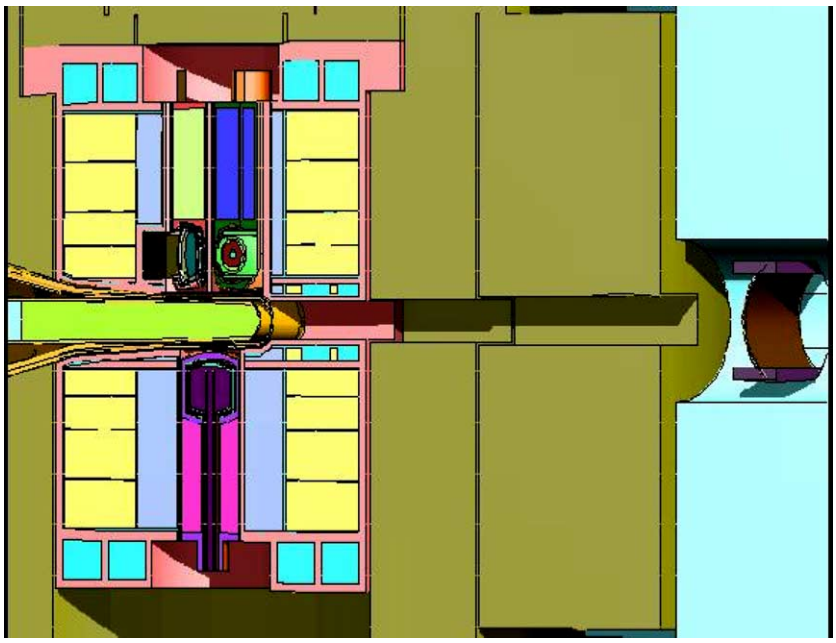

Fig. 5. Schematic 3D-view of target–moderator–reflector assembly (vertical cross-section view along proton-beam axis).

Table 2
Main parameters of calculation model

Item	Calculation condition
Proton-beam	
Power	1 MW at proton-beam window
Operation time	5000 h/year
Profile	Emittance: 81πmm mrad Gaussian + uniform (see Fig. 6) Footprint: 180×70 mm^2
Repetation rate	25 Hz
Proton-beam window	
Material and thickness	A5083, 2.5 mm$^t \times 2$ plates
Target	
Material	Mercury
Vessel material	316L stainless steel
Moderator	
Material	Super-critical hydrogen, 20 K
Vessel material	A6061-T6
Reflector	
Material and sizes (inner)	Be, ϕ 500×1000 mm^2
Material and sizes (outer)	Iron, ϕ 1000×1000 mm^2
Coolant material, fraction	D_2O, 5%
Water-cooled shield	
Material	316L stainless steel
Coolant material, fraction	H_2O, 10%
Middle section	
Material	316L Stainless steel
Coolant material, fraction	H_2O, 10%

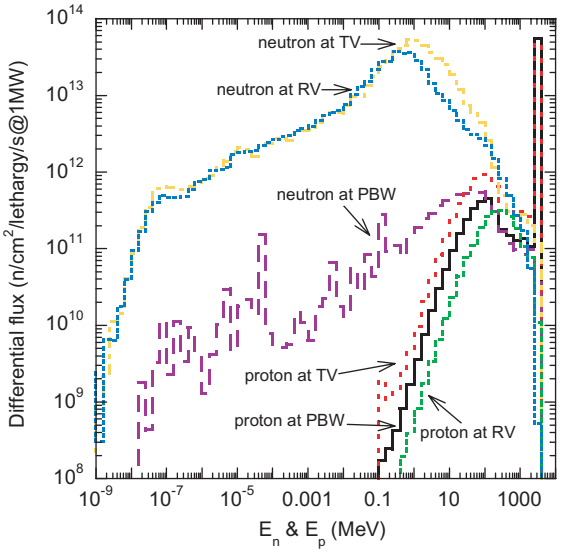

Fig. 7. Energy spectra (time averaged fluxes) for neutrons and protons at various important regions (at maximum DPA region). PBW: Proton-beam window; TV: Target vessel (entrance window) and RV: Reflector vessel (near target region).

important factors which determine the life of a moderator, due to the burn-up of those components. In a Hg container vessel, the pitting damage is the major factor which determines the mercury container vessel life. The role of the present paper is to discuss whether the DPA values during the design life are well within the maximum acceptable DPA values for each component. The maximum DPA values are listed in the sixth column in Table 4, which were determined from the irradiation data [21–24] and required mechanical strengths for each component. For example, in case of a hydrogen moderator vessel made of A6061-T6, the complete lost of the uniform elongation occurred at about 25 DPA [21,22]. The calculated stress level under the service condition of 1.5 MPa (design pressure 2.1 MPa) is about 60 MPa. This requires a uniform elongation of about 0.5 % at the end of the service life. We determined, from these considerations, the maximum acceptable DPA to be about 20 DPA. If those values for major components are determined as listed in the sixth column, the calculated values of the total DPA over design lives (fifth column) are smaller than the maximum acceptable DPA.

The distributions of calculated DPA values in the proposed model are depicted in Figs. 8 and 9 as

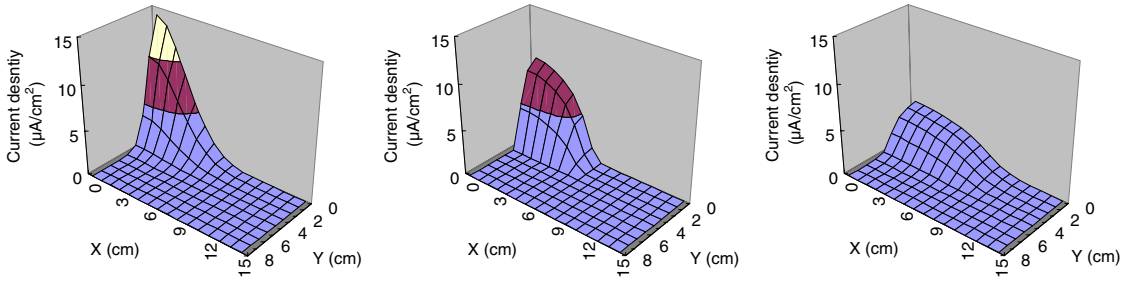

Fig. 6. Two-dimensional current densities for various proton-beam profiles. (Case 1) Footprint: 13×5 cm^2, Gaussian in phase space; (Case 2) Footprint: 13×5 cm^2, uniform in phase space; (Case 3) Footprint: 18×7 cm^2, uniform + Gaussian in phase space (adopted in the present JSNS design).

Table 3
Maximum DPA values for each component

Component	Position of maximum value	Maximum DPA (DPA/5000 MW h)			
		Total	Proton	Neutron	Rutherford scattering
Target					
Target container vessel	Center of front window	3.9	0.81	3.09	0.18
Inner water-cooled containment shroud	Center of front window	2.2	0.84	1.36	0.13
Outer water-cooled containment shroud	Center of front window	2.2	0.84	1.36	0.11
Reflector					
Reflector vessel	Center of vessel nearest target	2.8	0.02	2.78	0.03
Moderator					
Coupled moderator vessel	Center of vessel nearest target	2.8	0.02	2.78	0.02
Proton-beam window					
Upstream window	Center of window	0.40	0.33	0.07	0.07
Downstream window	Center of window	0.44	0.34	0.1	0.06
Water-cooled shield					
Vessel	Around proton-beam entrance hole	0.16	0.00	0.16	0.00
Middle-section					
Vessel	Around proton-beam entrance hole	0.04	0.01	0.03	0.00

Table 4
Calculated DPA, design life and the maximum acceptable DPA for each component

Component	Material	Maximum DPA (DPA/5000 MW h)	Design life (year[a])	Total DPA over design life (DPA)	Maximum acceptable DPA (DPA)
Target					
Target container vessel	316L stainless	3.9	0.5	2.0	5
Reflector					
Reflector vessel	A6061-T6	2.8	6	16.8	20
Moderator					
Coupled moderator vessel	A6061-T6	2.8	6	16.8	20
Proton-beam window					
Downstream window	A5083	0.44	>10	4.4	10
Water-cooled shield					
Vessel	316L stainless	0.16	>30	4.8	10
Middle section					
Vessel	316L stainless	0.04	>30	4.8	10

[a] 1 MW × 5000 h operation is assumed per 1 year.

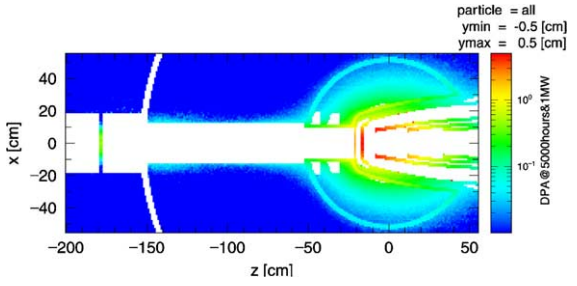

Fig. 8. DPA map of target–moderator–reflector assembly at horizontal plane through proton-beam center.

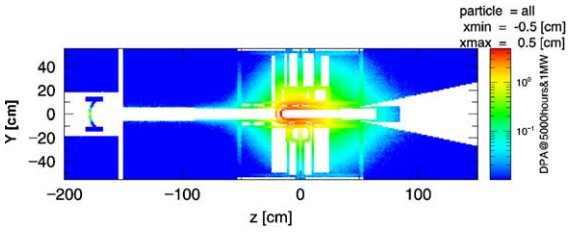

Fig. 9. DPA map of target–moderator–reflector assembly at vertical plane through proton-beam center.

Table 5
Comparison of the maximum DPA values for various beam profiles

Case	Peak current density	Maximum DPA (DPA/5000 MW h)			
	($\mu A/cm^2$)	Proton-beam window	Target container vessel	Reflector vessel	Moderator vessel
1	14.0	1.3	8.8	3.2	3.2
2	9.8	0.9	7.0	3.0	3.0
3	4.3	0.4	3.9	2.8	2.8

Table 6
Dependence of the maximum DPA on proton-energy

Case[a]	Peak current density	Maximum DPA (DPA/5000 MW h)			
	($\mu A/cm^2$)	Proton-beam window	Target container vessel	Reflector vessel	Moderator vessel
3	4.3	0.4	3.9	2.8	2.8
4	13.0	1.3	6.7	3.4	3.4

[a] Proton-beam condition per MW: Case 3: 3 GeV and 0.333 mA in total, Case 4: 1 GeV, 1 mA in total.

two-dimensional DPA maps. As apparent in the figures, the DPA values near the target are the highest.

Table 5 shows the DPA dependence on proton-beam profile. The DPA values of the moderator and the reflector vessels are almost independent of proton-beam condition, since those are mainly determined by neutrons. However, the DPA values of the target container vessel and the proton-beam window largely depend on the proton-current density, since the proton contributions in case 3 are about 83% and 40% for the proton-beam window and the front (incident) window of the target vessel, respectively (see Table 3). These ratio is consistent with calculations for SNS [25,26].

Table 6 shows the proton-beam energy dependence on DPA. Proton energies are 3 GeV for the case 3 and 1 GeV for the case 4. The proton-beam profile and the power are the same for the both cases. The DPA values of the target vessel and the proton-beam window in case 4 are greater than those in case 3. This is because those components receive proton directly (lower the proton energy the higher the proton-beam current for a given beam power). However, the DPA values in the moderator and reflector vessel are almost the same in case 3 and case 4.

4. Discussions

The DPA values can not be determined in experiments. However, there exists a finite difference between the calculated $\sigma_{DX}(E)$ in the present study and those reported by other groups. For example, in SNS, spallation neutron source in USA, the DPA values after 5000 MW h operation are reported to be 10 for target vessel and four for moderator vessel [27]. Of course, there are some differences in the proton-beam energy, the proton-current density, the calculation code, and so on. However, the present DPA values are very consistent with those evaluated for SNS, taking into account the difference in proton-beam energy and current density. The important thing is that, in the prediction of DPA in the source design, we have to use the same code and $\sigma_{DX}(E)$ with those used for the analyses of irradiation experiments. An acceptable DPA limit must be judged from the mechanical properties of a respective material after irradiation based on the same DPA evaluation.

As shown in Fig. 2, the proton-energy dependence on $\sigma_{DX}(E)$ of ^{27}A1 and ^{56}Fe for GeV protons is rather small compared those at lower energies. Considering that the proton-energy dependence above 1 GeV is almost unchanged, for a given proton-beam power, a high proton energy is more acceptable as far as DPA is concerned.

The prediction of hydrogen and helium in structural materials is also an important issue. We simply report, here, those values without detail discussions. From the present calculation using PHITS, we found that hydrogen and helium production rates in JSNS are 470 appm H/DPA and 50 appm He/DPA for the target vessel, 40 appm H/DPA and 4 appm He/DPA for the moderator and reflector vessel, respectively. The present production rates are well consistent with reported values for SNS [27]. Calculations with the GEM mode, which is used in PHITS, gave a good agreement with experiments of the production of light atoms such as H and He [28].

The production of silicon in aluminum alloy is also an important issue. It is known that the silicon production occurs via a neutron capture reaction of ^{27}Al and a beta decay of ^{28}A1 to ^{28}Si. However, we do not discuss this issue in details in the present paper. The silicon production rate in the moderator and reflector vessel is about

280 appm Si/DPA (780 appm Si/5000 MW h) in JSNS. When compared with the SNS calculations [27], the production rates are within ±20% per DPA, i.e. the present results are consistent with the SNS calculations.

Acknowledgements

The authors would like to thank the staff of 'Information Systems Operating Division' in Japan Atomic Energy Research Institute for arrangements and operations of 'PC cluster', parallel calculation system.

The authors would also like to thank members of Neutron Facility Group in Japan Atomic Energy Research Institute for help.

References

[1] H. Iwasa, K. Niita, T. Nakamura, J. Nucl. Sci. Technol. 39 (2002) 1142.
[2] K. Niita et al., Nucl. Instrum. and Meth. B 184 (2001) 406.
[3] J.F. Briesmeister (Ed.), MCNP™ – A General Monte Carlo *N*-Particle Transport Code, Version 4C, LA-13709-M, Los Alamos, National Laboratory, 2000.
[4] K. Iga, H. Takada, Y. Ikeda, Displacement cross-section and DPA calculation using NMTC/JAM, JAERI-Tech. 99-023, Japan Atomic Energy Research Institute, 1999 (in Japanese).
[5] R.E. MacFarlane, D.W. Muir, The NJOY Nuclear Data Processing System Version 91, LA-12740-M, Los Alamos, National Laboratory, 1994.
[6] M.J. Norgett, M.T. Robinson, I.T. Torrens, Nucl. Eng. Des. 33 (1974) 50.
[7] 1992 Annual Books of ASTM Standards, vol. 12.02, E521-89, E693-79, 1992.
[8] M.B. Chadwick, P.G. Young, S. Chiba, et al., Nucl Sci. Eng. 131 (1999) 293.
[9] J. Lindhard, V. Nielsen, M. Scharff, Mater. Fys. Medd. Dan. Vid. Selsk. 36 (10) (1963).
[10] T. Nakagawa et al., J. Nucl. Sci. Technol. 32 (1995) 1259.
[11] R.E. Prael, D.G. Madland, The LAHET Code System with LAHET2.8, LA-UR-00-2140, Los Alamos, National Laboratory, 2000.
[12] S. Meigo, K. Niita, S. Furihata, Analysis of residual nuclide distribution for Au(p,x) and Pb(p,x) with NMTC/JAM, AESJ C45, Iwaki, Fukishima, Japan, 14–16 September 2002.
[13] Yu.A. Korovin et al., Nucl. Instrum. and Meth. A 463 (2001) 544.
[14] K. Niita, private communication, 2003.
[15] S. Furihata, K. Niita, S. Meigo, Y. Ikeda, F. Maekawa, The GEM code. A simulation program for the evaporation and the fission process of an excited nucleus, JAERI-Data/Code 2001-015, Japan Atomic Energy Research Institute, 2001.
[16] K. Niita, S. Meigo, H. Takada, Y. Ikeda, High energy particle transport code NMTC/JAM, JAERI-Data/Code, 2001-007, Japan Atomic Energy Research Institute, 2001.
[17] H. Nakashima et al., J. Nucl. Sci. Technol. 2 (2002) 1155.
[18] F. Maekawa et al., Nucl. Sci. Eng., to be published.
[19] Materials Science Society of Japan, Irradiation Effects in Materials, 1994 (in Japanese).
[20] H. Kogawa, S. Ishikura, H. Sato, M. Harada, S. Takatama, M. Futakawa, K. Haga, R. Hino, S. Meigo, F. Maekawa, Y. Ikeda, Effect of proton beam profile on stress in JSNS target vessel, in: Proceedings of the IWSMT-6, in press.
[21] J.A. Dunlap et al., Effect Radiat. Mater., ASTM STP 1270 (1996) 1047.
[22] K. Farrel, R.T. King, Effects Radiat. Struct. Mater., ASTM STP 683 (1979) 440.
[23] K. Kikuchi, S. Saito, Y. Nishio and K. Usami, Post-Irradiation tensile and fatigue experiment, in: JPCA Sixth International Meeting on Nuclear Applications of Accelerator Technology (AccApp'03), San Diego, 2003, p. 874.
[24] Y. Dai, Suitability of steels as ESS mercury target container materials, in: 4th Plenary Meeting of European Spallation Source, 1995, p. 604.
[25] P.D. Ferguson et al., Radiation damage in aluminum proton beam Windows for SNS, in: Proceedings of the Acc/App/ADTTA'01, ANS (CD-ROM), 2002.
[26] M.H. Barnett et al., J. Nucl. Mater. 296 (2001) 54.
[27] P.D. Ferguson et al., Radiation damage calculations for the SNS target and moderators vessels and reflector system, presented in IWSMT-6, 2004.
[28] S. Furihata, Nucl. Instrum. and Meth. B 171 (2000) 251.